Supporting Information

Centimeter-Sized Single Crystals of 3D perovskitoid (4-AP)Pb_2X_6 (X = Br, I) for Efficient and Stable X-ray Detection

Hongliang Dai,[a] Zeng-Kui Zhu,*[b] Shihai You,[c] Junhua Luo*[c]

[a] School of Chemistry and Chemical Engineering, Key Laboratory of Jiangxi Province for Special Optoelectronic Artificial Crystal Materials, Jinggangshan University, Ji'an, Jiangxi, 343009, China
[b] College of Chemistry and Materials
Jiangxi Province Key Laboratory of Porous Functional Materials; Jiangxi Normal University, Nanchang, Jiangxi, 330022, China. E-mail: zkzhu@jxnu.edu.cn
[c] State Key Laboratory of Functional Crystals and Devices
Fujian Institute of Research on the Structure of Matter, Chinese Academy of Sciences, Fuzhou, Fujian, 350002, China. E-mail: jhluo@fjirsm.ac.cn

Materials 4-Amidinopyridinium (4-AP) chloride (98%, Aladdin); lead acetate trihydrate ($Pb(Ac)_2·3H_2O$, 99.5%, Aladdin), hydrobromic acid (HBr, 48%, Aladdin), hydroiodic acid (HI, 55-57%, Aladdin). All the chemicals were bought and used without further purification.

Synthesis Crystalline materials of (4-AP)Pb_2Br/I_6 were obtained from saturated HBr/I solution (45 mL) containing stoichiometric amounts of $Pb(Ac)_2•3H_2O$ (4 mmol, 1.516 g) and corresponding 4-Amidinopyridinium (4-AP) chloride (1 mmol, 0.157 g). The saturated solution was then heated and stirred for 30 min at 100℃ to get the clear solution. With the solution temperature decreasing to saturated status, microcrystals were obtained by spontaneous nucleation. Bulk crystals were grown by slowly cooling (1℃/day) the above solution from 80℃ to 30℃.

Powder X-ray diffraction Powder X-ray diffraction (PXRD) was recorded on a Rigaku MiniFlex diffractometer at room temperature. The diffraction patterns were collected in the 2θ range of 5°-50° with a step size of 0.02°. The experimental PXRD patterns match fairly well with the simulated data based on the single-crystal structure, which confirm the pure phase of (4-AP)Pb_2Br/I_6 (Fig. S1-2). For the sample after exposed to ambient air for 90 days, it shows environmental stability with negligible phase change. (Fig. 2d-e)

Thermogravimetric analysis (TGA) measurement TGA was performed on STA449C Thermal Analyser ranging from the room temperature to 1000℃ (Fig. 1c).

Single-crystal structure determination: Single-crystal X-ray diffraction was performed on a Bruker 8 diffractometer with the Mo Kα radiation. The data were processed by the Crystalclear software package. The structures were solved by direct methods and then refined by the full-matrix least-squares refinements on F2 using SHELXLTL software package. Crystallographic data and structure refinements for (4-AP)Pb_2Br/I_6 are given in Table S1.

X-ray detection The I-V traces and I-t curves under X-ray irradiation were recorded using the 6517B high precision electrometer (Keithley, USA). A commercially available Ag target X-ray tube with X-ray photons energy up to 50 keV and peak intensity at 22 keV was used as the X-ray source (4 W, Mini-X2, Amptek, USA). The dose rate of X-ray tube was modulated by changing its tube current and measured by a commercial X-ray dosimeter (Accu-Gold, Radcal, USA) attached with the ion chamber (10X6-180 model) in an integrating mode.

Calculations of mobility lifetime product (μτ) the $\mu\tau$ product has been extracted by fitting the voltage-dependent photoconductivity under X-ray irradiation with the standard Hecht equation,

$$I = \frac{I_0 \mu\tau V}{L^2}\left[1 - exp\left(-\frac{L^2}{\mu\tau V}\right)\right]$$

where I is the photocurrent, I_0 is the saturated photocurrent, L is the electrode spacing (1 mm for both A and B detectors), V is the bias voltage, μ is carrier mobility, and τ is carrier lifetime.

Calculations of sensitivity (S) and signal-to-noise ratio (SNR) S is defined as the collected charge per unit area under X-ray irradiation and can be determined by

$$S = (I_{x\text{-}ray} - I_d) / (D \times A)$$

where $I_{x\text{-}ray}$ and I_d are the currents recorded under X-ray irradiation and in the dark, respectively, D is the irradiation dose rate, and A is the effective area of detector.

SNR is calculated by

$$SNR = (I_{x\text{-}ray} - I_d)/ I_{noise}$$

where I_{noise} is the noise current and is obtained by calculating the standard deviation of the $I_{x\text{-}ray}$.

Calculation of Dark Current Drift (I_{drift}) The dark current drift is determined by the following equation

$$I_{drift} = (I_t - I_0) / (E \times S \times t)$$

where I_0 is the current immediately after stabilization, I_t is the current at time t, E is the electric field, S is the device area.

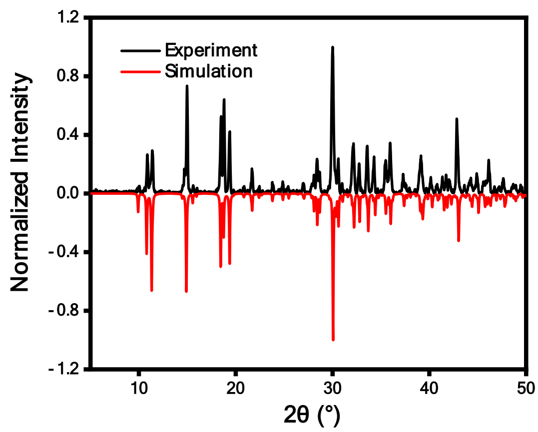

Fig. S1 Experimental and simulated powder X-ray diffraction patterns of $(4\text{-}AP)Pb_2Br_6$.

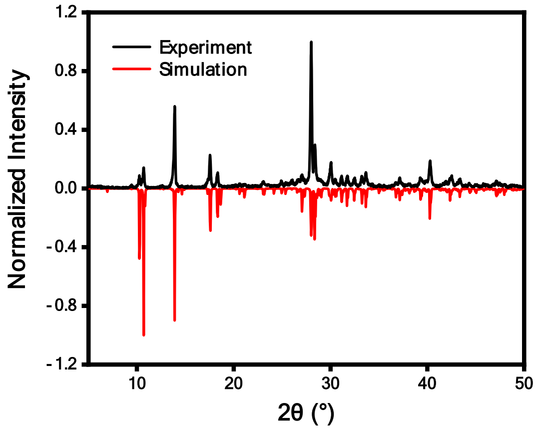

Fig. S2 Experimental and simulated powder X-ray diffraction patterns of (4-AP)Pb_2I_6.

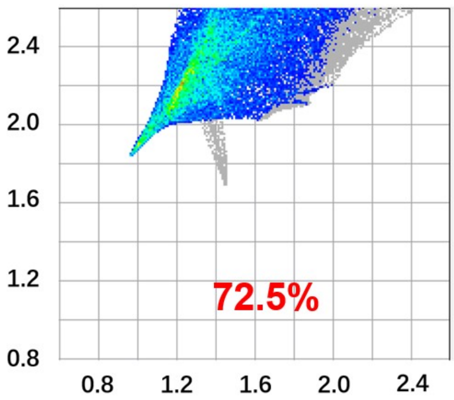

Fig. S3 2D fingerprint plots for 4-AP^{2+} cations in (4-AP)Pb_2I_6.

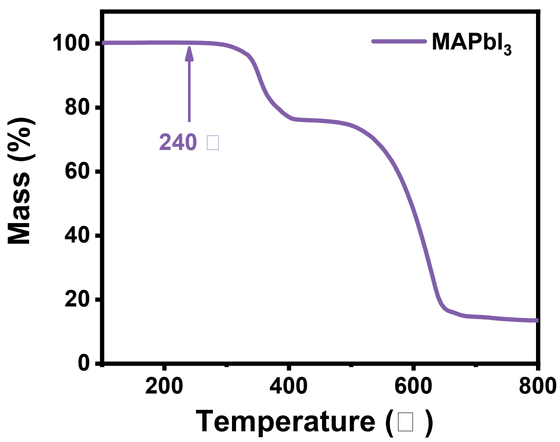

Fig. S4 The thermogravimetric cure of $MAPbI_3$.

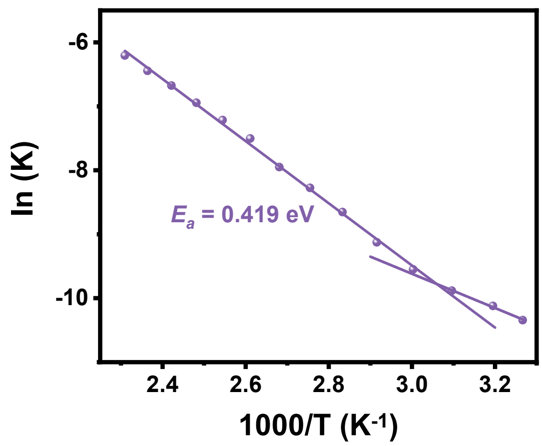

Fig. S5 Temperature-dependent conductivity of $MAPbI_3$ SC.

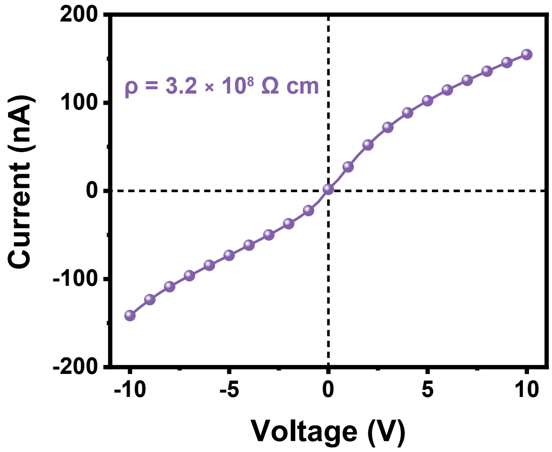

Fig. S6 Resistivity of $MAPbI_3$ SC.

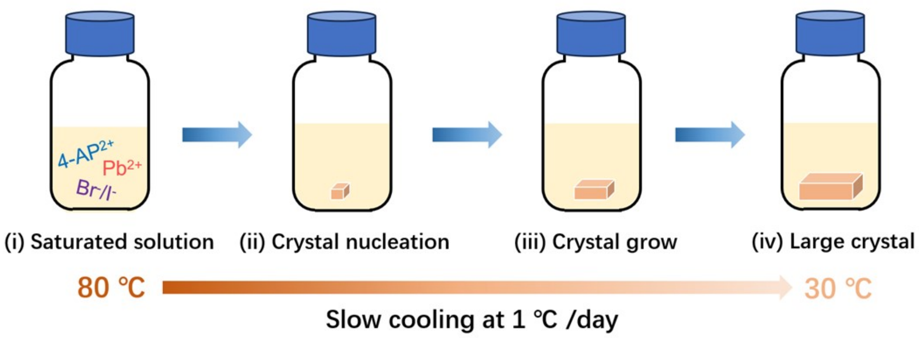

Fig. S7 Schematic diagram of the crystal growth process.

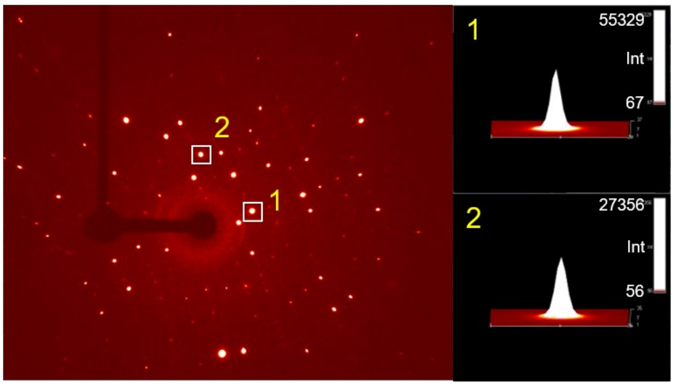

Fig. S8 SCXRD diffraction spots of (4-AP)Pb_2I_6.

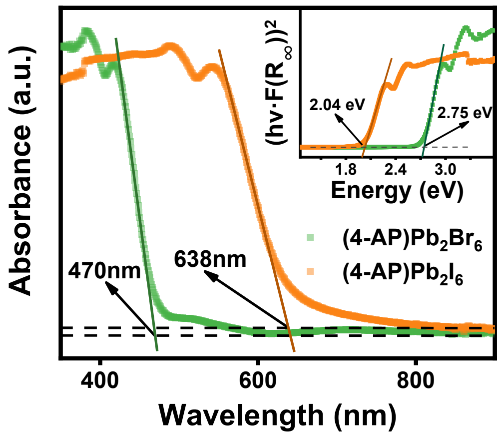

Fig. S9 UV–vis absorption spectra of (4-AP)Pb_2Br_6 and (4-AP)Pb_2I_6. Insert: the energy band estimated by a Tauc's plot.

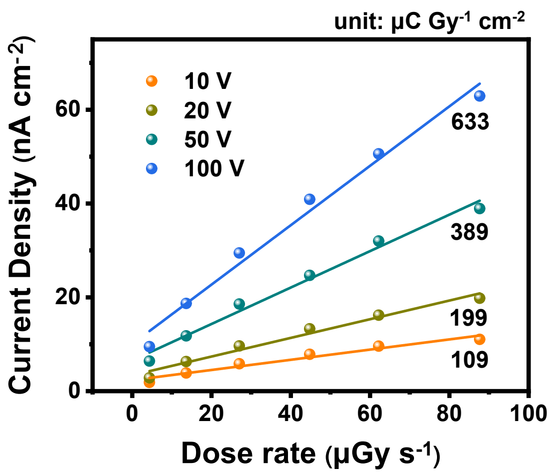

Fig. S10 Photocurrent density of (4-AP)Pb_2Br_6 detectors under various dose rates at different bias voltage.

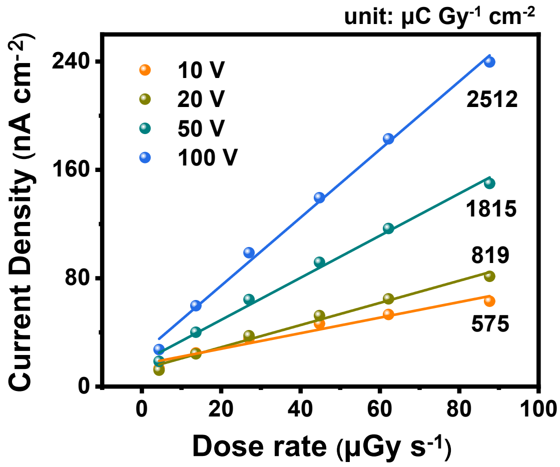

Fig. S11 Photocurrent density of (4-AP)Pb_2I_6 detectors under various dose rates at different bias voltage.

Table S1. Crystallographic Data and Structure Refinements of (4-AP)Pb_2Br/I_6.

	(4-AP)Pb_2Br_6	(4-AP)Pb_2I_6
CCDC Identification code	2312099	2312100
Empirical formula	$C_6H_9Br_6N_3Pb_2$	$C_6H_8I_6N_3Pb_2$
Formula weight	1008.068	1297.93
Temperature/K	295.00(10)	295.00(10)
Crystal system	orthorhombic	orthorhombic
Space group	*Pnna*	*Pnna*
a/Å	23.9011(15)	25.5050(12)
b/Å	15.7772(10)	16.5271(9)
c/Å	9.6867(5)	10.0933(6)
α/°	90	90
β/°	90	90
γ/°	90	90
Volume/Å^3	3652.8(4)	4254.6(4)
Z	8	8
ρ_{calc}g/cm^3	3.666	4.053
μ/mm^{-1}	31.525	24.503
F(000)	3399.3	4376.0
Radiation	Mo $K\alpha$ (λ = 0.71073)	Mo $K\alpha$ (λ = 0.71073)
2Θ range for data collection/°	6.82 to 57.68	6.57 to 57.634
Index ranges	$-31 \le h \le 26$, $-19 \le k \le 18$, $-10 \le l \le 12$	$-29 \le h \le 33$, $-18 \le k \le 22$, $-13 \le l \le 10$
Reflections collected	17692	17964
Independent reflections	4042 [R_{int} = 0.0459, R_{sigma} = 0.0391]	4758 [R_{int} = 0.0408, R_{sigma} = 0.0366]
Data/restraints/parameters	4042/0/157	4758/0/157
Goodness-of-fit on F^2	1.061	1.054
Final R indexes [$I >= 2\sigma(I)$]	R_1 = 0.0352, wR_2 = 0.0731	R_1 = 0.0419, wR_2 = 0.0917
Final R indexes [all data]	R_1 = 0.0615, wR_2 = 0.0867	R_1 = 0.0640, wR_2 = 0.1038

Table S2. Performances of some reported MHP and perovskitoid X-ray single-crystal detectors.

Materials	Dimensionality	Sensitivity ($\mu C\ Gy^{-1}\ cm^{-2}$)	Detection limit ($nGy\ s^{-1}$)	Current drift ($nA\ cm^{-1}\ s^{-1}\ V^{-1}$)	Ref.
$(4\text{-}AP)Pb_2Br_6$ $(4\text{-}AP)Pb_2I_6$	3D	633 2512	14900 720	3.1×10^{-6} 1.48×10^{-5}	**This work**
$Cs_2AgBiBr_6$	3D	1974	45.7	-	[1]
$CsPbBr_3$	3D	46180	10.81	1.68×10^{-6}	[2]
$MAPbI_3$	3D	5.2×10^6	0.1	-	[3]
$MAPbBr_3$	3D	96000	2.8	-	[4]
$FAPbBr_3$	3D	185.64	133	-	[5]
$CsFAGAPb(I_{0.9}Br_{0.1})_3$: Sr	3D	26000	7.09	8.77×10^{-5}	[6]
$FAPbBr_3$	3D	130	300	-	[7]
$(3AMPY)Pb_2I_6$	3D	207	-	-	[8]
$MhyPbBr_3$	3D	220 (0 V) 514 (100 V)	203 5428	0 5.77×10^{-5}	[9]
(*R*/*S*-BPEA)$EA_6Pb_4Cl_{15}$	3D	1709.09	3500	-	[10]
$([Cu(O_2C\text{-}(CH_2)_3\text{-}NH_3)_2]PbBr_4$	2D	1.14×10^5	56	-	[11]
$(BZA)_2(MA)Pb_2Br_7$	2D	97.9	266	3.9×10^{-6}	[12]
$(CH_3OC_3H_9N)_2CsPb_2Br_7$	2D	410	-	-	[13]
$BA_2EA_2Pb_3I_{10}$	2D	5555.7	17.2	9.25×10^{-6}	[14]
$(4ABA)PbI_4$	2D	150	7.5	5.18×10^{-8}	[15]
$(BA)_2PbI_4$	2D	204	241	-	[16]
$(PMA)_2PbI_4$	2D	283	2130	-	[17]
$(F\text{-}PEA)_2PbI_4$	2D	3402	23	4.9×10^{-8}	[18]
$(o\text{-}F\text{-}PEA)_2PbI_4$	2D	1724.5	460	8.48×10^{-8}	[19]
(*S*-BPEA)$_2FAPb_2I_7$	2D	87.8 1985.9	161 1100	- 4.4×10^{-7}	[20]
$(2IPA)_2FAPb_2I_7$	2D	438	20	7.76×10^{-6}	[21]
(1,3-BMACH)$(MA)Pb_2I_7$	2D	199	106	-	[22]
$BDAPbI_4$	2D	242	430	6.06×10^{-9}	[23]
(1,3-BMACH)BiI_5	1D	170	49	-	[22]
$(BZA)_2$(*R*/*S*-PPA)BiI_6	1D	53.2 2170	18.5 -	- -	[24]
$(BAH)BiI_4$	1D	1181.8	77	-	[25]
$MA_3Bi_2I_9$	0D	1947	83	5.0×10^{-10}	[26]
(*R*/*S*-PPA)$_2BiI_5$	0D	31 150 (10 V)	270	0 1.40×10^{-4}	[27]
$(HIS)BiI_5$	0D	1230	36.4	2.559×10^{-7}	[28]

Reference

[1] L. Yin, H. Wu, W. Pan, B. Yang, P. Li, J. Luo, G. Niu, J. Tang, *Adv. Opt. Mater.* **2019**, 7, 1900491.

[2] Y. Hua, G. Zhang, X. Sun, X. Li, Z. Zhai, F. Cui, J. Liu, H. Liu, X. Tao, *Nat. Photonics* **2024**, 18, 870-877.

[3] Y. Song, L. Li, M. Hao, W. Bi, A. Wang, Y. Kang, H. Li, X. Li, Y. Fang, D. Yang, Q. Dong, *Adv. Mater.* **2021**, 33, 2103078.

[4] W. Zhang, H. Wang, Z. Chen, P. Wang, X. Liu, H. Dong, J. Zhao, Y. Cui and Y. Shao, *ACS Appl. Mater. Interfaces*, **2024**, 16, 12844-12852.

[5] M. Girolami, F. Matteocci, S. Pettinato, V. Serpente, E. Bolli, B. Paci, A. Generosi, S. Salvatori, A. Di Carlo and D. M. Trucchi, Nano-Micro Letters, 2024, 16, 182.

[6] J. Jiang, M. Xiong, K. Fan, C. Bao, D. Xin, Z. Pan, L. Fei, H. Huang, L. Zhou, K. Yao, X. Zheng, L. Shen, F. Gao, *Nat. Photonics* **2022**, 16, 575-581.

[7] M. Yao, J. Jiang, D. Xin, Y. Ma, W. Wei, X. Zheng, L. Shen, *Nano Lett.* **2021**, 21, 3947-3955.

[8] X. Li, Y. He, M. Kepenekian, P. Guo, W. Ke, J. Even, C. Katan, C. C. Stoumpos, R. D. Schaller, M. G. Kanatzidis, *J. Am. Chem. Soc.* **2020**, 142, 6625-6637.

[9] Q. Guan, S. You, Z.-K. Zhu, R. Li, H. Ye, C. Zhang, H. Li, C. Ji, X. Liu, J. Luo, *Angew. Chem. Int. Ed.* **2024**, 63, e202320180.

[10] Q. Guan, T. Zhu, Z. K. Zhu, H. Ye, S. You, P. Xu, J. Wu, X. Niu, C. Zhang, X. Liu, J. Luo, *Angew. Chem. Int. Ed.* **2023**, 62, e202307034.

[11] K. Guo, W. Li, Y. He, X. Feng, J. Song, W. Pan, W. Qu, B. Yang, H. Wei, *Angew. Chem. Int. Ed.* **2023**, 62, e202303445.

[12] J. Li, T. Zhu, H. Ye, Q. Guan, S. You, R. Li, Y. Geng, J. Luo, *Small* **2024**, DOI: 10.1002/smll.2024015452401545.

[13] C. Ji, Y. Li, X. Liu, Y. Wang, T. Zhu, Q. Chen, L. Li, S. Wang, J. Luo, *Angew. Chem. Int. Ed.* **2021**, 60, 20970-20976.

[14] Y. Jiang, C. Zhang, Z. K. Zhu, J. Wu, P. Yu, Y. Zeng, H. Ye, H. Dai, R. Li, Q. Guan, G. Chen, H. Yang, J. Luo, *Angew. Chem. Int. Ed.* **2024**, 63, e202407305.

[15] Q. Fan, Y. Ma, S. You, H. Xu, W. Guo, Y. Liu, L. Tang, W. Li, J. Luo, Z. Sun, *Adv. Funct. Mater.* **2023**, 34, 2312395.

[16] Yukta, J. Ghosh, M. A. Afroz, S. Alghamdi, P. J. Sellin, S. Satapathi, *ACS Photonics* **2022**, 9, 3529-3539.

[17] C.-X. Qian, M.-Z. Wang, S.-S. Lu, H.-J. Feng, *Appl. Phys. Lett.* **2022**, 120, 011901.

[18] H. Li, J. Song, W. Pan, D. Xu, W. A. Zhu, H. Wei, B. Yang, *Adv. Mater.* **2020**, 32, 2003790.

[19] B. Zhang, Z. Xu, C. Ma, H. Li, Y. Liu, L. Gao, J. Zhang, J. You, S. Liu, *Adv. Funct. Mater.* **2022**, 32, 2110392.

[20] Q. Guan, H. Ye, S. You, Z. K. Zhu, H. Li, X. Liu, J. Luo, *Small* **2023**, 20, e2307908.

[21] S. You, P. Yu, J. Wu, Z. K. Zhu, Q. Guan, L. Li, C. Ji, X. Liu, J. Luo, *Adv. Sci.* **2023**, 10, 2301149.

[22] D. Fu, Z. Chen, Y. Chang, X.-M. Zhang, *Chem. Mater* **2023**, 35, 9806-9816.

[23] Y. Shen, Y. Liu, H. Ye, Y. Zheng, Q. Wei, Y. Xia, Y. Chen, K. Zhao, W. Huang, S. Liu, *Angew. Chem. Int. Ed.* **2020**, 59, 14896-14902.

[24] Z. K. Zhu, T. Zhu, S. You, P. Yu, J. Wu, Y. Zeng, Q. Guan, Z. Li, C. Qu, H. Zhong, L. Li, J. Luo, *Small* **2023**, 20, e2307454.

[25] C. Ma, H. Li, M. Chen, Y. Liu, K. Zhao, S. Liu, *Adv. Funct. Mater.* **2022**, 32, 2202160.

[26] Y. Liu, Z. Xu, Z. Yang, Y. Zhang, J. Cui, Y. He, H. Ye, K. Zhao, H. Sun, R. Lu, M. Liu, M. G. Kanatzidis, S. Liu, *Matter* **2020**, 3, 180-196.

[27] S. You, Z. K. Zhu, S. Dai, J. Wu, Q. Guan, T. Zhu, P. Yu, C. Chen, Q. Chen, J. Luo, *Adv. Funct. Mater.* **2023**, 33, 2303523.

[28] Z. Zhao, Q. Fan, Y. Liu, H. Rong, H. Ni, L. Wei, X. Zhao, J. Luo, Z. Sun, *ACS Appl. Mater. Interfaces* **2024**, 16, 38283-38289.